Available online at www.sciencedirect.com
SCIENCE DIRECT
Journal of Sound and Vibration 294 (2006) 314–328
JOURNAL OF SOUND AND VIBRATION
www.elsevier.com/locate/jsvi

A robust control method for seismic protection of civil frame building

Jong-Cheng Wu[a,*], Hsin-Hsien Chih[b], Chern-Hwa Chen[c]

[a]*Department of Civil Engineering, Tamkang University, Taipei, Taiwan*
[b]*Department of Civil Engineering, Tamkang University, Taipei, Taiwan*
[c]*Department of Civil and Environmental Engineering, National University of Kaohsiung, Kaohsiung, Taiwan*

Received 15 March 2004; received in revised form 4 November 2005; accepted 19 November 2005
Available online 7 February 2006

Abstract

Recently, more and more experimental studies indicate that a mature active control design toward practical implementation requires consideration of robustness criteria in the design process, which includes the performance robustness in reducing tracking error and in resistance to external disturbance and measurement noise, and the stability robustness with respect to system uncertainty. In this paper, a robust control method employing these robustness criteria that can be further converted to a generalized H_∞ control problem is presented for control of civil structures. To facilitate computation of H_∞ controllers, an efficient solution procedure based on linear matrix inequalities (LMI), the so-called LMI-based H_∞ control, is introduced. For verifying applicability of the proposed method, extensive simulations were conducted on a numerical building model with active bracings under seismic excitation, which was constructed from a full-scale steel frame building that was once tested on a shake table. In the simulation, system uncertainty is assumed in the controller design and the use of acceleration feedback is emphasized for practical consideration. From the simulation results, it is demonstrated that the performance of H_∞ controllers proposed is remarkable and robust, and the efficiency of LMI-based approach is also approved. Therefore, this robust control method is suitable for application to seismic protection of civil frame buildings.

1. Introduction

Over the past two decades, the use of active control on civil engineering structures for suppression of seismic- and wind-induced vibrations has attracted a great deal of attention because of its remarkable effectiveness (e.g., Refs. [1–3]). Considerable research efforts on the experimental verification using shake table tests and wind tunnel tests have been made and presented in several literatures (e.g., Refs. [4–9] etc.). The valuable experience gained through these tests indicates that a mature active control design toward practical implementation requires the consideration of robustness criteria in the design process, that is, the performance robustness in reducing the tracking error, in resistance to the external disturbance and measurement noise, and the stability robustness with respect to the existence of system uncertainty [10]. In particular, the stability

*Corresponding author. Tel.: +886 226215656; fax: +886 226209747.
E-mail address: jcwu@bridge.ce.tku.edu.tw (J.-C. Wu).

0022-460X/$ - see front matter © 2006 Elsevier Ltd. All rights reserved.
doi:10.1016/j.jsv.2005.11.019

robustness to uncertainty is relatively important in the stage of controller design because the properties of most civil structures are not easy to be precisely predicted. Among the advanced control strategies proposed in many literatures (e.g. Refs. [2,3]), H_∞ control strategy is particularly useful in designing the robust controller because these robustness criteria in a way can be interpreted as the H_∞ norm of a transfer function to be smaller than a given value.

The solution method for computing H_∞ controllers has been broadly discussed in the control community since the past decades (e.g., Refs. [10–13]). Among all, two typical literatures, i.e., Refs. [12,13], presented a numerically efficient methodology by solving two algebraic Riccati equations. However, its application is restricted to the so-called regular control system (i.e., $\mathbf{D}_{12}$ and $\mathbf{D}_{21}$ in Eqs. (4) and (5) of the later sections have full column ranks). Later, a new methodology based on the solution of linear matrix inequalities (LMI), which can be directly derived from the Bounded Real Lemma, was proposed by Gahinet and Apkarian [14], and termed as the LMI-based H_∞ control. The theorem of the LMI-based solution method is more straightforward and no restriction is required. Besides, this solution procedure is quite efficient in terms of computation.

Based on these understandings, in this paper, an H_∞ control method that takes the robustness criteria into account will be proposed using the LMI-based solution procedure. For demonstration, a numerical model of a full-scale seismic-excited building was used to conduct numerical simulation for verifying its applicability toward implementation on civil engineering structures. This full-scale building considered herein is made of a three-story spatial steel rigid frame and equipped with an active bracing system on the first floor (see Fig. 8 in the numerical simulation section). It was once constructed on the shake table of the National Center for Research on Earthquake Engineering (NCREE), Taiwan for verification of active control. This numerical model of the building was constructed and presented in Ref. [7] and its validity has been well verified through shake table tests. By the fact shown in Ref. [7], this numerical model was esteemed to be suitably used for numerical simulation to verify other control methods to be employed. In addition, the comparisons with the numerical results using the linear quadratic Gaussian (LQG) control were also made for demonstration of their control performance.

2. Formulation

In this section, we will first describe the basic concept of generalized H_∞ control for a controlled system, followed by a brief description of the LMI-based procedures for solving H_∞ controllers proposed by Gahinet and Apkarian [14]. Secondly, the concept of robustness criteria in a form of H_∞ norm is introduced for controlling a physically seismic-excited structure. Thirdly, the formulation of forming an H_∞ control problem that takes these robustness criteria into account will be derived in a way that the LMI-based procedures can be utilized in consequence.

2.1. Generalized H_∞ control

A typical block diagram of a generalized H_∞ controlled system is shown in Fig. 1. The generalized plant system is denoted by $\mathbf{G}(s)$ which has two sets of inputs $\mathbf{W}$ and $\mathbf{U}$, and two sets of outputs $\mathbf{z}$ and $\mathbf{y}$. In Fig. 1, the

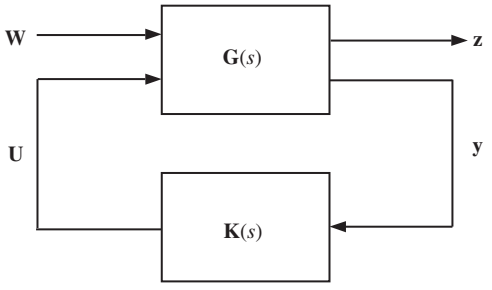

Fig. 1. Block diagram of a generalized H_∞ control problem.

m_1-dimensional vector $\mathbf{W}$ is the exogenous input, which might involve the external disturbance, measurement noise or reference signal, while the m_2-dimensional vector $\mathbf{U}$ is the control command from a controller. The p_1-dimensional vector $\mathbf{z}$ that contains the physical quantities to be attenuated is referred to as the controlled output, while the p_2-dimensional vector $\mathbf{y}$ that contains the measurements to be used as the feedback quantities is referred to as the measured output. The block denoted by $\mathbf{K}(s)$ represents the transfer function of a dynamic output feedback controller to be designed. In the concept of H_∞ control, the objective is to design an appropriate dynamic output feedback controller $\mathbf{K}(s)$ such that the transfer function from $\mathbf{W}$ to $\mathbf{z}$, denoted as $\mathbf{H}_{\mathbf{zw}}$, is stable and its H_∞ norm, denoted by $\|\mathbf{H}_{\mathbf{zw}}\|_\infty$, is smaller than a given attenuation value γ, i.e., $\|\mathbf{H}_{\mathbf{zw}}\|_\infty < \gamma$. The H_∞ norm of the transfer function $\mathbf{H}_{\mathbf{zw}}$ is defined as

$$\|\mathbf{H}_{\mathbf{zw}}\|_\infty = \operatorname*{Sup}_{\mathbf{W}(t)\in R} \frac{\|\mathbf{z}(t)\|_2}{\|\mathbf{W}(t)\|_2}, \tag{1}$$

where $\|.\|_2 = (\int_0^\infty (.)^{\mathrm{T}}(.)\,\mathrm{d}t)^{1/2}$ is the L_2 norm of a time-variant vector. In other words, the H_∞ norm is the worst case of the ratio of output's L_2 norm versus input's L_2 norm. Therefore, the condition $\|\mathbf{H}_{\mathbf{zw}}\|_\infty < \gamma$ obviously implies $\|\mathbf{z}(t)\|_2 < \gamma \|\mathbf{W}(t)\|_2$. It can be easily shown that the H_∞ norm in Eq. (1) for a linear system can be equivalently expressed as

$$\|\mathbf{H}_{\mathbf{zw}}\|_\infty = \operatorname*{Sup}_{\omega\in R} \bar{\sigma}(\mathbf{H}_{\mathbf{zw}}(\mathrm{j}\omega)), \tag{2}$$

in which $\mathrm{j} = \sqrt{-1}$ and $\bar{\sigma}(.)$ denotes the largest singular value.

In the state space, the generalized plant $\mathbf{G}(s)$ can be represented by a state equation expressed by

$$\dot{\mathbf{X}} = \mathbf{A}\mathbf{X} + \mathbf{B}_1\mathbf{W} + \mathbf{B}_2\mathbf{U}, \tag{3}$$

$$\mathbf{z} = \mathbf{C}_1\mathbf{X} + \mathbf{D}_{11}\mathbf{W} + \mathbf{D}_{12}\mathbf{U}, \tag{4}$$

$$\mathbf{y} = \mathbf{C}_2\mathbf{X} + \mathbf{D}_{21}\mathbf{W} + \mathbf{D}_{22}\mathbf{U}, \tag{5}$$

in which $\mathbf{A} \in R^{n\times n}$, $\mathbf{B}_1 \in R^{n\times m_1}$, $\mathbf{B}_2 \in R^{n\times m_2}$, $\mathbf{C}_1 \in R^{p_1\times n}$, $\mathbf{D}_{11} \in R^{p_1\times m_1}$, $\mathbf{D}_{12} \in R^{p_1\times m_2}$, $\mathbf{C}_2 \in R^{p_2\times n}$, $\mathbf{D}_{21} \in R^{p_2\times m_1}$, $\mathbf{D}_{22} \in R^{p_2\times m_2}$; $(\mathbf{A}, \mathbf{B}_2)$ is stabilizable and $(\mathbf{A}, \mathbf{C}_2)$ is detectable. Likely, the state equation of the controller $\mathbf{K}(s)$ can be expressed by

$$\dot{\mathbf{X}}_\mathbf{k} = \mathbf{A}_\mathbf{k}\mathbf{X}_\mathbf{k} + \mathbf{B}_\mathbf{k}\mathbf{y}, \tag{6}$$

$$\mathbf{U} = \mathbf{C}_\mathbf{k}\mathbf{X}_\mathbf{k} + \mathbf{D}_\mathbf{k}\mathbf{y}, \tag{7}$$

in which $\mathbf{A}_\mathbf{k} \in R^{k\times k}$, $\mathbf{B}_\mathbf{k} \in R^{k\times p_2}$, $\mathbf{C}_\mathbf{k} \in R^{m_2\times k}$, $\mathbf{D}_\mathbf{k} \in R^{m_2\times p_2}$ are constant matrices to be determined by a control theory. For simplifying the following derivation, another measured output $\bar{\mathbf{y}} = \mathbf{y} - \mathbf{D}_{22}\mathbf{U} = \mathbf{C}_2\mathbf{X} + \mathbf{D}_{21}\mathbf{W}$ instead of $\mathbf{y}$ is firstly used in Eqs. (6) and (7). This assumption will be eliminated later by a simple transformation described in the subsequent section. Thus, the corresponding matrices for the controller in Eqs. (6) and (7) shall be replaced by $\bar{\mathbf{A}}_\mathbf{k}, \bar{\mathbf{B}}_\mathbf{k}, \bar{\mathbf{C}}_\mathbf{k}, \bar{\mathbf{D}}_\mathbf{k}$, respectively. Hence, the closed-loop transfer function $\mathbf{H}_{\mathbf{zw}}$ can be obtained by substituting Eq. (7) into Eq. (4) as

$$\mathbf{H}_{\mathbf{zw}}(s) = \mathbf{D}_{\mathbf{cl}} + \mathbf{C}_{\mathbf{cl}}(s\mathbf{I} - \mathbf{A}_{\mathbf{cl}})^{-1}\mathbf{B}_{\mathbf{cl}}, \tag{8}$$

$$\mathbf{A}_{\mathbf{cl}} = \mathbf{A}_0 + \boldsymbol{\beta}\boldsymbol{\theta}\boldsymbol{\varsigma}, \quad \mathbf{B}_{\mathbf{cl}} = \mathbf{B}_0 + \boldsymbol{\beta}\boldsymbol{\theta}\boldsymbol{\zeta}_{21}, \quad \mathbf{C}_{\mathbf{cl}} = \mathbf{C}_0 + \boldsymbol{\zeta}_{12}\boldsymbol{\theta}\boldsymbol{\varsigma}, \quad \mathbf{D}_{\mathbf{cl}} = \mathbf{D}_{11} + \boldsymbol{\zeta}_{12}\boldsymbol{\theta}\boldsymbol{\xi}_{21}, \tag{9}$$

in which

$$\mathbf{A}_0 = \begin{bmatrix} \mathbf{A} & 0 \\ 0 & 0_\mathbf{k} \end{bmatrix}, \quad \mathbf{B}_0 = \begin{bmatrix} \mathbf{B}_1 \\ 0 \end{bmatrix}, \quad \mathbf{C}_0 = [\mathbf{C}_1 \;\; 0], \quad \boldsymbol{\beta} = \begin{bmatrix} 0 & \mathbf{B}_2 \\ \mathbf{I}_\mathbf{k} & 0 \end{bmatrix}, \quad \boldsymbol{\varsigma} = \begin{bmatrix} 0 & \mathbf{I}_\mathbf{k} \\ \mathbf{C}_2 & 0 \end{bmatrix},$$

$$\boldsymbol{\zeta}_{12} = [\,0 \quad \mathbf{D}_{21}\,], \quad \boldsymbol{\zeta}_{21} = \begin{bmatrix} 0 \\ \mathbf{D}_{21} \end{bmatrix}, \quad \boldsymbol{\theta} = \begin{bmatrix} \bar{\mathbf{A}}_\mathbf{k} & \bar{\mathbf{B}}_\mathbf{k} \\ \bar{\mathbf{C}}_\mathbf{k} & \bar{\mathbf{D}}_\mathbf{k} \end{bmatrix}. \tag{10}$$

In Eq. (10), $0_\mathbf{k}$ represents a $(k \times k)$-dimensional matrix with all 0 entries and $\mathbf{I}_\mathbf{k}$ represents a $(k \times k)$-dimensional identity matrix.

2.2. LMI-based solution procedure

According to the bounded real lemma (e.g., Refs. [14,10]), a controller $\mathbf{K}(s)$ in Fig. 1 that satisfies the condition of $\|\mathbf{H}_{zw}\|_\infty < \gamma$ exists if and only if there exists a symmetric matrix $\mathbf{X}_{cl} \in R^{(n+k)\times(n+k)} > 0$ (i.e., $\mathbf{X}_{cl}$ is positive definite) such that

$$\begin{bmatrix} \mathbf{A}_{cl}^{T}\mathbf{X}_{cl} + \mathbf{X}_{cl}\mathbf{A}_{cl} & \mathbf{X}_{cl}\mathbf{B}_{cl} & \mathbf{C}_{cl}^{T} \\ \mathbf{B}_{cl}^{T}\mathbf{X}_{cl} & -\gamma\mathbf{I} & \mathbf{D}_{cl}^{T} \\ \mathbf{C}_{cl} & \mathbf{D}_{cl} & -\gamma\mathbf{I} \end{bmatrix} < 0. \tag{11}$$

In other words, the controller matrices $(\bar{\mathbf{A}}_k, \bar{\mathbf{B}}_k, \bar{\mathbf{C}}_k, \bar{\mathbf{D}}_k,)$ and a positive definitive $\mathbf{X}_{cl}$ that satisfy inequality (11) can be found if and only if $\|\mathbf{H}_{zw}\|_\infty < \gamma$. Inequality (11) can be further rewritten as

$$\mathbf{\Psi}_{\mathbf{X}_{cl}} + \boldsymbol{\psi}^{T}\boldsymbol{\theta}^{T}\boldsymbol{\xi}_{\mathbf{X}_{cl}} + \boldsymbol{\xi}_{\mathbf{X}_{cl}}^{T}\boldsymbol{\theta}\boldsymbol{\psi} < \mathbf{0}, \tag{12}$$

in which

$$\mathbf{\Psi}_{\mathbf{X}_{cl}} = \begin{bmatrix} \mathbf{A}_0^{T}\mathbf{X}_{cl} + \mathbf{X}_{cl}\mathbf{A}_0^{T} & \mathbf{X}_{cl}\mathbf{B}_0 & \mathbf{C}_0^{T} \\ \mathbf{B}_0^{T}\mathbf{X}_{cl} & -\gamma\mathbf{I} & \mathbf{D}_{11}^{T} \\ \mathbf{C}_0 & \mathbf{D}_{11} & -\gamma\mathbf{I} \end{bmatrix}, \tag{13}$$

$$\boldsymbol{\psi} = [\boldsymbol{\varsigma},\ \boldsymbol{\zeta}_{21},\ 0_{(k+p_2)\times p_1}], \quad \boldsymbol{\xi}_{\mathbf{X}_{cl}} = [\boldsymbol{\beta}^{T}\mathbf{X}_{cl},\ 0_{(k+m_2)\times m_1},\ \boldsymbol{\zeta}_{12}^{T}].$$

Note that inequality (12) is an LMI for either $\boldsymbol{\theta}$ or $\mathbf{X}_{cl}$ individually, but not for both. By partitioning $\mathbf{X}_{cl}$ and $\mathbf{X}_{cl}^{-1}$ as

$$\mathbf{X}_{cl} = \begin{bmatrix} \mathbf{S} & \mathbf{N} \\ \mathbf{N}^{T} & * \end{bmatrix}, \quad \mathbf{X}_{cl}^{-1} = \begin{bmatrix} \mathbf{R} & \mathbf{M} \\ \mathbf{M}^{T} & * \end{bmatrix}, \tag{14}$$

in which $\mathbf{R}, \mathbf{S} \in R^{n\times n}$; $\mathbf{M}, \mathbf{N} \in R^{n\times k}$, and employing the projection lemma [14], several manipulations for inequality (12) lead to two LMIs for $\mathbf{R}$ and $\mathbf{S}$ (the detail derivation is described in Appendix A for the reader's interest), i.e.,

$$\begin{bmatrix} \mathbf{N}_R & 0 \\ 0 & \mathbf{I}_{m_1} \end{bmatrix}^{T} \begin{bmatrix} \mathbf{AR} + \mathbf{RA}^{T} & \mathbf{RC}_1^{T} & \mathbf{B}_1 \\ \mathbf{C}_1\mathbf{R} & -\gamma\mathbf{I} & \mathbf{D}_{11} \\ \mathbf{B}_1^{T} & \mathbf{D}_{11}^{T} & -\gamma\mathbf{I} \end{bmatrix} \begin{bmatrix} \mathbf{N}_R & 0 \\ 0 & \mathbf{I}_{m_1} \end{bmatrix} < 0, \tag{15}$$

$$\begin{bmatrix} \mathbf{N}_S & 0 \\ 0 & \mathbf{I}_{p_1} \end{bmatrix}^{T} \begin{bmatrix} \mathbf{AS} + \mathbf{A}^{T}\mathbf{S} & \mathbf{SB}_1^{T} & \mathbf{C}_1^{T} \\ \mathbf{B}_1^{T}\mathbf{S} & -\gamma\mathbf{I} & \mathbf{D}_{11} \\ \mathbf{B}_1^{T} & \mathbf{D}_{11}^{T} & -\gamma\mathbf{I} \end{bmatrix} \begin{bmatrix} \mathbf{N}_R & 0 \\ 0 & \mathbf{I}_{p_1} \end{bmatrix} < 0, \tag{16}$$

in which $\mathbf{N}_R$ and $\mathbf{N}_S$ are the null base matrices of $[\mathbf{B}_2^{T}\ \ \mathbf{D}_{21}^{T}]$, and $[\mathbf{C}_2\ \ \mathbf{D}_{21}]$, respectively. In addition, the positive definiteness of $\mathbf{X}_{cl}$ equivalently leads to another LMI for $\mathbf{R}$ and $\mathbf{S}$ as

$$\begin{bmatrix} \mathbf{R} & \mathbf{I} \\ \mathbf{I} & \mathbf{S} \end{bmatrix} \geqslant 0 \tag{17}$$

[15]. Hence, Eqs. (15)–(17) are the three basic LMIs for solving H_∞ controllers.

Finally, the LMI-based solution procedure for the H_∞ controller can be summarized in the following:

(i) Use Matlab LMI Toolbox to solve γ, $\mathbf{R}$ and $\mathbf{S}$ by constructing a minimization problem with an objective function J expressed by

$$J = \gamma + \alpha\,\mathrm{Trace}(\mathbf{R}) + \beta\,\mathrm{Trace}(\mathbf{S}), \tag{18}$$

which is subject to three LMI constraints described in inequalities (15)–(17). In addition, one more constraint expressed as

$$\gamma > 0.5\gamma_{\min} \tag{19}$$

can be also used to restrict the value of γ. In Eq. (18), α, β are two specified weightings to modulate the trace of $\mathbf{R}$ and $\mathbf{S}$, and the parameter $\gamma_{\min}$ in Eq. (19) is given to confine the lower bound of γ. Minimization of the traces of $\mathbf{R}$ and $\mathbf{S}$ is helpful in slowing down the dynamics of the controller for facilitating implementation.

(ii) From the identity

$$\mathbf{M}\mathbf{N}^{\mathrm{T}} = \mathbf{I} - \mathbf{R}\mathbf{S}, \tag{20}$$

which is actually induced from Eq. (14), the matrices $\mathbf{M}, \mathbf{N} \in R^{n\times k}$ in full column rank can be obtained by using the singular value decomposition. Thus, by substituting $\mathbf{M}$ and $\mathbf{N}$ into an identity

$$\begin{bmatrix} \mathbf{S} & \mathbf{I} \\ \mathbf{N}^{\mathrm{T}} & 0 \end{bmatrix} = \mathbf{X}_{\mathbf{cl}} \begin{bmatrix} \mathbf{I} & \mathbf{R} \\ 0 & \mathbf{M}^{\mathrm{T}} \end{bmatrix}, \tag{21}$$

which can be also deduced from Eq. (14), the matrix $\mathbf{X}_{\mathbf{cl}} \in R^{(n+k)\times(n+k)}$ can be obtained.

(iii) Construct a minimization problem with an objective function

$$J = \mathrm{Trace}(\bar{\mathbf{A}}_{\mathbf{k}}), \tag{22}$$

subject to the LMI constraint described in inequality (12), by using the Matlab LMI Toolbox to solve the controller matrices $\bar{\mathbf{A}}_{\mathbf{k}} \in R^{k\times k}$, $\bar{\mathbf{B}}_{\mathbf{k}} \in R^{k\times p_2}$, $\bar{\mathbf{C}}_{\mathbf{k}} \in R^{m_2\times k}$, $\bar{\mathbf{D}}_{\mathbf{k}} \in R^{m_2\times p_2}$ in the matrix $\boldsymbol{\theta}$.

(iv) Once $\bar{\mathbf{A}}_{\mathbf{k}}$, $\bar{\mathbf{B}}_{\mathbf{k}}$, $\bar{\mathbf{C}}_{\mathbf{k}}$, $\bar{\mathbf{D}}_{\mathbf{k}}$ are obtained, the assumption of using measured output $\bar{\mathbf{y}} = \mathbf{y} - \mathbf{D}_{22}\mathbf{U} = \mathbf{C}_2\mathbf{X} + \mathbf{D}_{21}\mathbf{W}$ to replace $\mathbf{y}$ is eliminated by a simple transformation, i.e.,

$$\begin{aligned} &\mathbf{A}_{\mathbf{k}} = \bar{\mathbf{A}}_{\mathbf{k}} - \bar{\mathbf{B}}_{\mathbf{k}}\mathbf{D}_{22}(\mathbf{I} + \bar{\mathbf{D}}_{\mathbf{k}}\mathbf{D}_{22})^{-1}\bar{\mathbf{C}}_{\mathbf{k}}, \quad \mathbf{B}_{\mathbf{k}} = \bar{\mathbf{B}}_{\mathbf{k}} - \bar{\mathbf{B}}_{\mathbf{k}}\mathbf{D}_{22}\left(\mathbf{I} + \bar{\mathbf{D}}_{\mathbf{k}}\mathbf{D}_{22}\right)^{-1}\bar{\mathbf{D}}_{\mathbf{k}}, \\ &\mathbf{C}_{\mathbf{k}} = (\mathbf{I} + \bar{\mathbf{D}}_{\mathbf{k}}\mathbf{D}_{22})^{-1}\bar{\mathbf{C}}_{\mathbf{k}}, \quad \mathbf{D}_{\mathbf{k}} = (\mathbf{I} + \bar{\mathbf{D}}_{\mathbf{k}}\mathbf{D}_{22})^{-1}\bar{\mathbf{D}}_{\mathbf{k}}. \end{aligned} \tag{23}$$

2.3. Robustness criteria in robust control

For completeness of the derivation for robustness criteria, the physical system considered in this section is restricted to the so-called matched system, i.e., the system excited by the control effort (command) $\mathbf{U}$ and disturbance $\mathbf{d}$ (earthquakes or wind loads) through the same mechanism. The block diagram of such a physical system with active control is shown in Fig. 2 by the part with solid borders and lines. For the unmatched systems to which most structural systems belong, these robustness requirements derived can be still applied, except that the performance will degrade to some degrees, depending on the situation.

In Fig. 2, the block $\mathbf{P}$ is the structural system (plant system); the block $\mathbf{K}$ is the controller system; $\mathbf{r}$ is the reference signal (to be used in a tracking problem); $\mathbf{U}$ is the control command generated from the controller; $\mathbf{d}$ is the external disturbance such as earthquake or wind loading; $\mathbf{n}$ is the measurement noise; $\mathbf{y}$ is the measured structural response; and $\mathbf{e}$ is the error signal which is the subtraction of the measured response from the reference. In vibration suppression problems, the reference $\mathbf{r}$ can be considered to be a zero signal and the

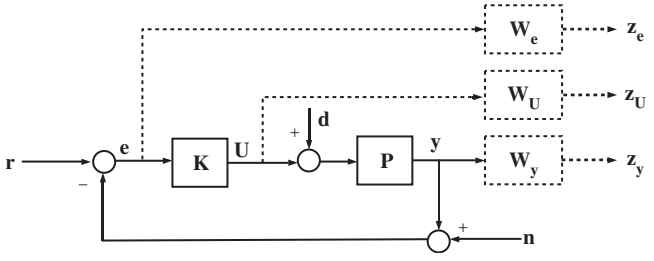

Fig. 2. Block diagram of a physical system with active control.

same block diagram applies. It can be easily shown that the following relations in the frequency domain can be derived from the block diagram in Fig. 2:

$$\mathbf{y} = \mathbf{T}_0(\mathbf{r} - \mathbf{n}) + \mathbf{S}_0\mathbf{P}\mathbf{d}, \tag{24}$$

$$\mathbf{e} = \mathbf{S}_0\mathbf{r} + \mathbf{T}_0\mathbf{n} - \mathbf{S}_0\mathbf{P}\mathbf{d}, \tag{25}$$

in which $\mathbf{S}_0$ is the so-called sensitivity function and $\mathbf{T}_0$ is the complimentary sensitivity function, defined respectively as

$$\mathbf{S}_0 = (\mathbf{I} + \mathbf{P}\mathbf{K})^{-1}, \quad \mathbf{T}_0 = (\mathbf{I} + \mathbf{P}\mathbf{K})^{-1}\mathbf{P}\mathbf{K}. \tag{26}$$

It is well understood that the robustness criteria considered in active control should contain both of performance robustness and stability robustness. As such, performance robustness may include resistance to the influence of reference **r** and disturbance **d**, and the influence of measurement noise **n** on the response **y** or error **e**. In a way, the "size" of influence in frequency domain can be somehow quantified by the ratio of L_2 norm of the output vector versus that of the input vector. This ratio at a certain frequency ω is mathematically bounded by the largest singular value of the corresponding transfer function, which is denoted by $\bar{\sigma}(.)$. It should be noted that the L_2 norm here simply means the L_2 norm for a constant vector, rather than the definition used in Eq. (1) for a time-variant vector. Therefore, the performance robustness for disturbance attenuation, tracking error reduction and noise rejection in robust control can be summarized as follows [10]:

(i) For maintaining performance of disturbance attenuation, the condition $\bar{\sigma}(\mathbf{H}_{\mathbf{yd}}(\omega)) \ll 1$ is required for $\forall\omega \in R$, i.e., $\bar{\sigma}(\mathbf{S}_0\mathbf{P}) \ll 1$ for $\forall\omega \in R$. Or, more conservatively, the condition $\bar{\sigma}(\mathbf{S}_0) \ll 1$ is required for $\forall\omega \in R$.
(ii) For maintaining performance of tracking error reduction, the condition $\bar{\sigma}(\mathbf{H}_{\mathbf{er}}(\omega)) \ll 1$ is required for $\forall\omega \in R$, i.e., $\bar{\sigma}(\mathbf{S}_0) \ll 1$ for $\forall\omega \in R$.
(iii) For maintaining performance of noise rejection, the condition $\bar{\sigma}(\mathbf{H}_{\mathbf{yn}}(\omega)) \ll 1$ is required for $\forall\omega \in R$, i.e., $\bar{\sigma}(\mathbf{T}_0) \ll 1$ for $\forall\omega \in R$.

Items (i) and (ii) indicate $\bar{\sigma}(\mathbf{S}_0) \ll 1$ for $\forall\omega \in R$, and item (iii) indicates $\bar{\sigma}(\mathbf{T}_0) \ll 1$ for $\forall\omega \in R$. However, from the relation $\mathbf{S}_0 + \mathbf{T}_0 = \mathbf{I}$, it is not possible to simultaneously achieve both conditions. Fortunately, since the dominant frequency distribution of the disturbance **d** used in (i) (or reference **r** used in (ii)) lies in the relatively low range and that of the noise **n** used in (iii) lies in the relatively high range (see the illustration in Fig. 3), by imposing the conditions $\bar{\sigma}(\mathbf{W}_\mathbf{e}\mathbf{S}_0) < 1$ and $\bar{\sigma}(\mathbf{W}_\mathbf{y}\mathbf{T}_0) < 1$ for $\forall\omega \in R$ with appropriate frequency-dependent weighting functions $\mathbf{W}_\mathbf{e}$ and $\mathbf{W}_\mathbf{y}$ which physically represents the frequency distribution of **d** (or **r**) and **n**, appropriate frequency distributions for $\bar{\sigma}(\mathbf{S}_0)$ and $\bar{\sigma}(\mathbf{T}_0)$ can thus be achieved. Consequently, the performance robustness for disturbance attenuation, tracking error reduction and noise rejection can be expressed as

$$\|\mathbf{W}_\mathbf{e}\mathbf{S}_0\|_\infty < 1, \tag{27}$$

$$\|\mathbf{W}_\mathbf{y}\mathbf{T}_0\|_\infty < 1. \tag{28}$$

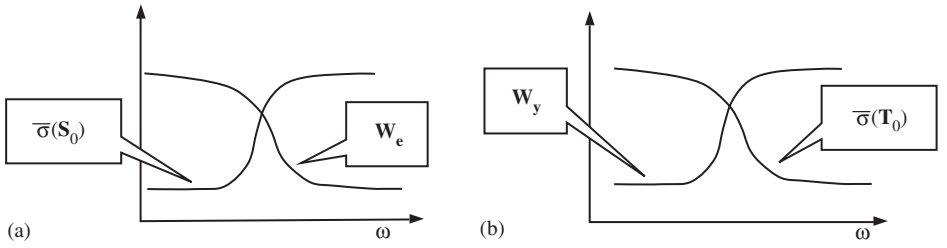

Fig. 3. Schematic diagram of frequency distribution: (a) $\bar{\sigma}(\mathbf{S}_0)$ and $\mathbf{W}_\mathbf{e}$; (b) $\bar{\sigma}(\mathbf{T}_0)$ and $\mathbf{W}_\mathbf{y}$.

Other than these, another issue concerned in robustness criteria is the stability robustness, which is the retaining stability in time with respect to system uncertainty. As mentioned in much literature (e.g., Ref. [10]), system uncertainties are mostly classified into multiplicative and additive uncertainties for convenience of discussion. Their effects on the system stability and the corresponding conditions for stability robustness are described in the following [10]:

(i) *Additive uncertainty*: A plant system with additive uncertainty can be represented by a set of transfer functions denoted by $\mathbf{\Pi} = \{\mathbf{P} + \mathbf{W}_U\mathbf{\Delta} : \mathbf{\Delta} \text{ is a stable transfer function of uncertainty}\}$, in which $\mathbf{W}_U$ is a weighting matrix for modulating the 'size' of Δ. For convenience of further discussion, Δ can be properly adjusted with $\|\Delta\|_\infty \leqslant 1$ to accommodate all possible uncertainties in the considered frequency range. The representation of additive uncertainty in the block diagram of a physical system is shown in Fig. 4. By means of the linear fractional transformation (LFT) technique, the block diagram in Fig. 4 can be converted into a simplified block diagram with an upper block Δ and a lower block $-\mathbf{W}_U\mathbf{K}\mathbf{S}_0$, as shown in Fig. 5. The derivation is shown as follows. Since the observation of $\mathbf{U} = \mathbf{K}\mathbf{e} = -\mathbf{K}\mathbf{y} = -\mathbf{K}(\mathbf{P}\mathbf{U} + \mathbf{o})$ from Fig. 4 leads to $\mathbf{U} = -(\mathbf{I} + \mathbf{K}\mathbf{P})^{-1}\mathbf{K}\mathbf{o}$, $\mathbf{i}$ can be expressed as $\mathbf{i} = -\mathbf{W}_U(\mathbf{I} + \mathbf{K}\mathbf{P})^{-1}\mathbf{K}\mathbf{o} = -\mathbf{W}_U\mathbf{K}(\mathbf{I} + \mathbf{P}\mathbf{K})^{-1}\mathbf{o} = -\mathbf{W}_U\mathbf{K}\mathbf{S}_0\mathbf{o}$. Furthermore, by the small gain theorem [10], the system stability is guaranteed if

$$\|\mathbf{W}_U\mathbf{K}\mathbf{S}_0\|_\infty < 1. \tag{29}$$

Hence, inequality (29) is a condition for stability robustness.

(ii) *Multiplicative uncertainty:* The plant system with the multiplicative uncertainty can be represented by a set denoted by $\mathbf{\Pi} = \{(\mathbf{I} + \mathbf{W}_y\mathbf{\Delta})\mathbf{P} : \mathbf{\Delta} \text{ is a stable transfer function of uncertainty}\}$, in which $\mathbf{W}_y$ is a weighting matrix for modulating the 'size' of Δ. Once again, Δ can be properly adjusted with $\|\Delta\|_\infty \leqslant 1$ to cover the bounds of all possible multiplicative uncertainties in the considered frequency range. The representation of multiplicative uncertainties in the block diagram of a physical system is shown in Fig. 6. By means of the technique of LFT, the block diagram in Fig. 6 can be converted into a simplified block diagram with an upper block Δ and a lower block $-\mathbf{W}_y\mathbf{T}_0$, as shown in Fig. 7. By the small gain theorem, it is concluded that the system stability is guaranteed if $\|\mathbf{W}_y\mathbf{T}_0\|_\infty < 1$, which is actually the same condition as inequality (28).

To summarize the concept described above, robustness criteria for active control should at least contain conditions of performance robustness and stability robustness expressed in inequalities (27)–(29). Conceptually, the transfer functions involved in these three conditions can be interpreted as the transfer functions from the reference $\mathbf{r}$ to $\mathbf{e}$, $\mathbf{U}$ and $\mathbf{y}$, multiplied by three weighting (filter) functions $\mathbf{W}_e$, $\mathbf{W}_U$ and $\mathbf{W}_y$, respectively. Following this idea, the controlled outputs considered herein become the three filtered quantities $\mathbf{z}_e$, $\mathbf{z}_U$ and $\mathbf{z}_y$, as illustrated by the block with dotted lines in Fig. 2.

2.4. Formulation of robust H_∞ control for civil structures

According to the ideas introduced in the previous sections, the remaining task is to convert the three robustness conditions expressed in inequalities (27)–(29) into a generalized H_∞ problem which will be presented in this section. Let us consider a civil structure with active control subject to external excitations. A matched system is used in the block diagram presented in Fig. 2 for constructing robust H_∞ controllers. Apparently, this is not the case for actual civil structures; degradation of control performance to some extent will be expected. First of all, the state equations of the plant system $\mathbf{P}$ (civil structure), weightings $\mathbf{W}_e$, $\mathbf{W}_U$ and

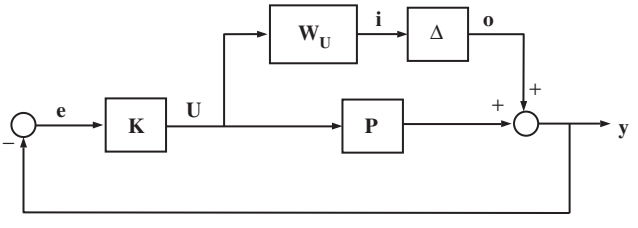

Fig. 4. Block diagram with additive uncertainty.

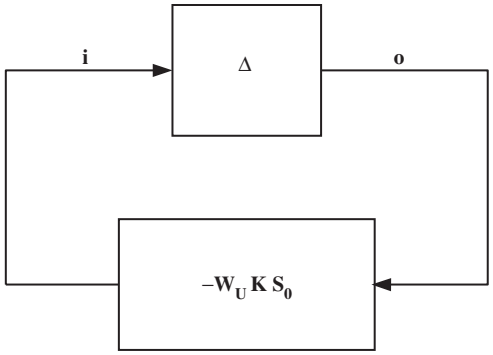

Fig. 5. Simplified block diagram with additive uncertainty after using LFT.

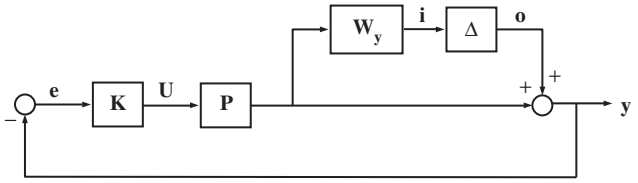

Fig. 6. Block diagram with multiplicative uncertainty.

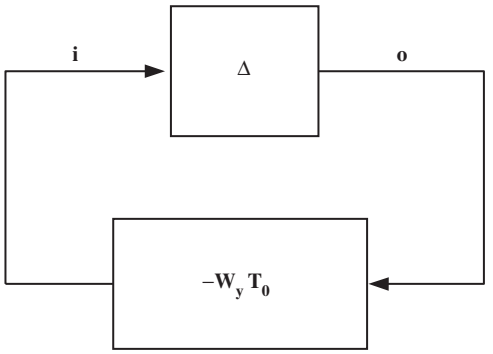

Fig. 7. Simplified block diagram with additive uncertainty after using LFT.

$\mathbf{W}_y$ are expressed by

$$\dot{\mathbf{X}}_P = \mathbf{A}_P\mathbf{X}_P + \mathbf{B}_P\mathbf{d} + \mathbf{E}_p\mathbf{U}, \quad \mathbf{y} = \mathbf{C}_P\mathbf{X}_P + \mathbf{D}_P\mathbf{d} + \mathbf{F}_P\mathbf{U}, \tag{30}$$

$$\dot{\mathbf{X}}_e = \mathbf{A}_e\mathbf{X}_e + \mathbf{B}_e\mathbf{e}, \quad \mathbf{z}_e = \mathbf{C}_e\mathbf{X}_e + \mathbf{D}_e\mathbf{e}, \tag{31}$$

$$\dot{\mathbf{X}}_U = \mathbf{A}_U\mathbf{X}_U + \mathbf{B}_U\mathbf{U}, \quad \mathbf{z}_U = \mathbf{C}_U\mathbf{X}_U + \mathbf{D}_U\mathbf{U} \tag{32}$$

and

$$\dot{\mathbf{X}}_y = \mathbf{A}_y\mathbf{X}_y + \mathbf{B}_y\mathbf{y}, \quad \mathbf{z}_y = \mathbf{C}_y\mathbf{X}_y + \mathbf{D}_y\mathbf{y}, \tag{33}$$

respectively, in which $\mathbf{X}_P$, $\mathbf{X}_e$, $\mathbf{X}_U$, $\mathbf{X}_y$ are the state vectors; $\mathbf{A}_P$, $\mathbf{B}_P$, $\mathbf{C}_P$, $\mathbf{D}_P$, $\mathbf{E}_P$, $\mathbf{F}_P$, $\mathbf{A}_e$, $\mathbf{B}_e$, $\mathbf{C}_e$, $\mathbf{D}_e$, $\mathbf{A}_U$, $\mathbf{B}_U$, $\mathbf{C}_U$, $\mathbf{D}_U$, $\mathbf{A}_y$, $\mathbf{B}_y$, $\mathbf{C}_y$ and $\mathbf{D}_y$ are constant matrices in the state equations with appropriate dimensions. Besides the transfer functions from $\mathbf{r}$ to $\mathbf{z}_e$, $\mathbf{z}_U$ and $\mathbf{z}_y$ that are to be constructed according to the robustness criteria in inequalities (27)–(29), it is esteemed necessary for vibration suppression to also include the transfer functions from the external disturbance $\mathbf{d}$ to $\mathbf{z}_e$, $\mathbf{z}_U$ and $\mathbf{z}_y$ for attenuation purpose. Thus, by considering $\mathbf{r}$ and $\mathbf{d}$ as the exogenous input $\mathbf{W}$, $\mathbf{z}_e$, $\mathbf{z}_U$ and $\mathbf{z}_y$ as the controlled output $\mathbf{z}$, and $\mathbf{e}$ as the measured output (because $\mathbf{e}$ is equal to $-\mathbf{y}$ when $\mathbf{r}$ is equal to 0), a generalized H_∞ control problem with control objective $\|\mathbf{H}_{zw}\|_\infty < \gamma$ can be

formed with state equations expressed by

$$\dot{\mathbf{X}} = \mathbf{A}\mathbf{X} + \mathbf{B}_1\mathbf{W} + \mathbf{B}_2\mathbf{U}, \quad \mathbf{z} = \mathbf{C}_1\mathbf{X} + \mathbf{D}_{11}\mathbf{W} + \mathbf{D}_{12}\mathbf{U}, \quad \mathbf{e} = \mathbf{C}_2\mathbf{X} + \mathbf{D}_{21}\mathbf{W} + \mathbf{D}_{22}\mathbf{U}, \tag{34}$$

in which

$$\mathbf{X} = \begin{bmatrix} \mathbf{X_P} \\ \mathbf{X_e} \\ \mathbf{X_U} \\ \mathbf{X_y} \end{bmatrix}, \quad \mathbf{W} = \begin{bmatrix} \mathbf{r} \\ \mathbf{d} \end{bmatrix}, \quad \mathbf{z} = \begin{bmatrix} \mathbf{z_e} \\ \mathbf{z_U} \\ \mathbf{z_y} \end{bmatrix}, \quad \mathbf{A} = \begin{bmatrix} \mathbf{A_P} & 0 & 0 & 0 \\ -\mathbf{B_e}\mathbf{C_P} & \mathbf{A_e} & 0 & 0 \\ 0 & 0 & \mathbf{A_U} & 0 \\ \mathbf{B_y}\mathbf{C_P} & 0 & 0 & \mathbf{A_y} \end{bmatrix}, \quad \mathbf{B}_1 = \begin{bmatrix} 0 & \mathbf{B_P} \\ \mathbf{B_e} & -\mathbf{B_e}\mathbf{D_P} \\ 0 & 0 \\ 0 & \mathbf{B_y}\mathbf{D_P} \end{bmatrix},$$

$$\mathbf{B}_2 = \begin{bmatrix} \mathbf{E_P} \\ -\mathbf{B_e}\mathbf{F_P} \\ \mathbf{B_U} \\ \mathbf{B_y}\mathbf{F_P} \end{bmatrix}, \quad \mathbf{C}_1 = \begin{bmatrix} -\mathbf{D_e}\mathbf{C_P} & \mathbf{C_e} & 0 & 0 \\ 0 & 0 & \mathbf{C_U} & 0 \\ \mathbf{D_y}\mathbf{C_P} & 0 & 0 & \mathbf{C_y} \end{bmatrix}, \quad \mathbf{D}_{11} = \begin{bmatrix} \mathbf{D_e} & -\mathbf{D_e}\mathbf{D_P} \\ 0 & 0 \\ 0 & \mathbf{D_y}\mathbf{D_P} \end{bmatrix}, \quad \mathbf{D}_{12} = \begin{bmatrix} -\mathbf{D_e}\mathbf{F_P} \\ \mathbf{D_U} \\ \mathbf{D_y}\mathbf{F_P} \end{bmatrix}, \tag{35}$$

$$\mathbf{C}_2 = [-\mathbf{C_P} \;\; 0 \;\; 0 \;\; 0], \quad \mathbf{D}_{21} = [\mathbf{I} \;\; -\mathbf{D_P}], \quad \mathbf{D}_{22} = -\mathbf{F_P}.$$

The comparison of Eq. (34) and Eqs. (3)–(5) shows their similarity, except that **y** in Eq. (5) is replaced by **e** for feedback. Thus, the LMI-based solution procedure introduced in the previous section can be used to design the robust H_∞ controller.

3. Numerical example

To demonstrate the applicability of the robust H_∞ controller presented to civil structures, extensive numerical simulations using a numerical model of a three-story full-scale seismic-excited building were conducted. The building has a rectangular shape with a floor area of 4.5 m × 3 m in each floor and a total height of 9 m (3 m for each story), which was once constructed on the shake table of NCREE for experimental verification (as shown in Fig. 8). The masses of the building from the bottom to top floors are 1144.16, 1144.16 and 1113.62 kgf s^2/m, respectively. An active bracing system is connected between the ground and the first floor to provide the active force to the building for seismic protection. This actively controlled building has once been tested using LQG control and the results were presented in Ref. [7]. In Ref. [7], the numerical model of this actively controlled building was successfully constructed and the experimental verification has been conducted to show its correctness. Therefore, this numerical model will be directly used as the true model system in the numerical simulation herein. The system matrices of this numerical model can be found in the web site URL http://www.ce.tku.edu.tw/~jcwu/research/ncree_analytical.html. In this true system, the available responses of the building include relative displacement x_i ($i = 1, 2, 3$) of each floor w.r.t. the ground, absolute acceleration $\ddot{x}_{ia}$ ($i = 1, 2, 3$) of each floor and the stroke x_f of the actuator. Two earthquakes, the 1940 El Centro (100 s) and 1995 Kobe (60 s) earthquakes, are used as the excitation sources. The amplitude of PGA (Peak Ground Acceleration) adjusted to 0.1 g is used in the simulation as in the previous tests performed in Ref. [7]. In fact, since controller designs presented herein are linear control designs, the results under different scales of excitation can be easily calculated by multiplying a proportional factor.

The building with zero control command has three natural frequencies and damping ratios equal to 7.363, 22.933 and 37.966 rad/s, and 1.38%, 2.46% and 1.32%, respectively. For comparison, the response quantities of the building with zero command under earthquakes are tabulated in Table 1, and referred to as the "No Control" case in what follows. In Table 1, "Peak" represents the peak value in the entire time history, while "rms" represents the root-mean-square values within the dominant period from 24 to 64 s for El Centro earthquake and 14 to 54 s for Kobe earthquake.

Since the displacement and velocity measurements are expensive in implementation, absolute accelerations of all three floors are chosen to be the feedback quantities, i.e., $\mathbf{y} = [\ddot{x}_{1a}, \ddot{x}_{2a}, \ddot{x}_{3a}]^{\mathrm{T}}$. However, all seven response quantities mentioned above will be computed. It should be noted that during the design stage, the eight-state nominal system used in Ref. [7] for LQG control is constructed through the well-known balanced-state

Fig. 8. Three-story full-scale building on the shake table of NCREE.

Table 1
Response quantities of actively controlled building with zero command (no control case)

	El Centro (PGA = 0.1 g)		Kobe (PGA = 0.1 g)	
(1)	Peak (2)	rms (3)	Peak (4)	rms (5)
x_1 (cm)	2.050	0.823	2.065	0.664
x_2 (cm)	4.592	1.766	4.493	1.428
x_3 (cm)	6.232	2.335	5.981	1.889
$\ddot{x}_{1a}$ (g)	0.171	0.051	0.216	0.040
$\ddot{x}_{2a}$ (g)	0.262	0.097	0.264	0.078
$\ddot{x}_{3a}$ (g)	0.371	0.127	0.375	0.103

reduction method [16] from another system model which is identified with less accuracy than the true system. The transfer functions of the response quantities due to the actuator command U for both the nominal system and true system are plotted in Fig. 9 to illustrate the difference. It is observed from Fig. 9 that the size of

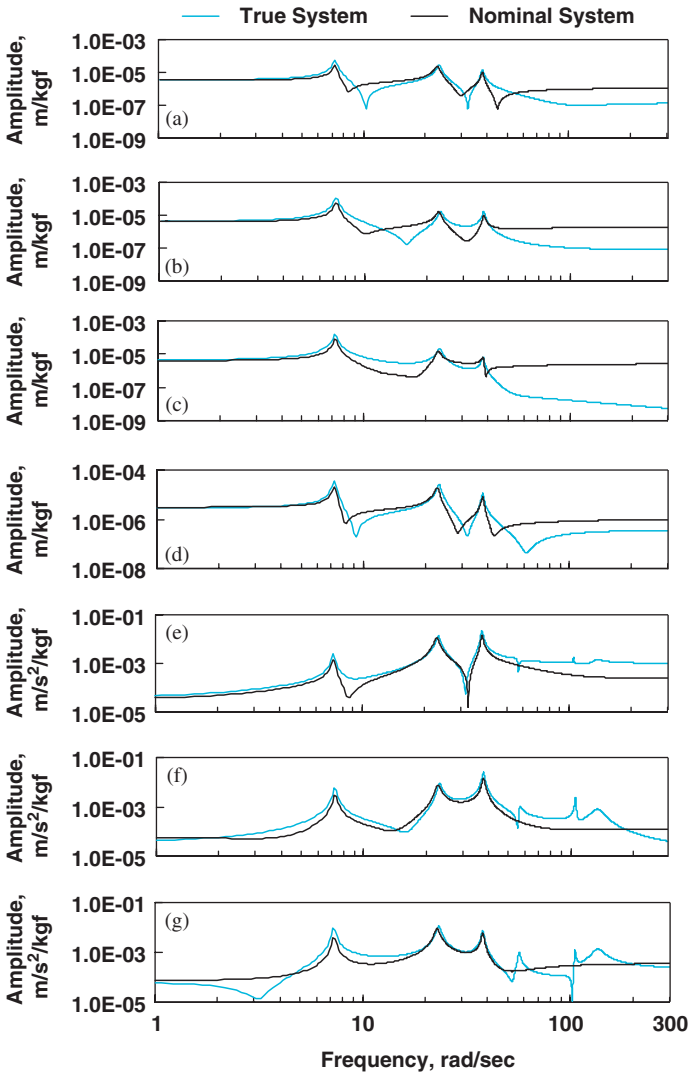

Fig. 9. Comparison of transfer functions of response quantities due to actuator command U: (a) x_1, (b) x_2, (c) x_3, (d) x_f, (e) $\ddot{x}_{1a}$, (f) $\ddot{x}_{2a}$, and (g) $\ddot{x}_{3a}$.

uncertainty from prediction error is more significant than that just induced from system reduction. The same nominal system is also used in this paper for the robust H_∞ controller design in order to examine robustness of the controller and make comparisons with the LQG results. Herein, the difference between the nominal system and the true system will be considered as the additive uncertainty and the weighting $\mathbf{W}_\mathbf{U}$ to be chosen should cover the bounds of all additive uncertainties.

In this study, two robust H_∞ controllers are designed, denoted as H_{∞_1} and H_{∞_2}, respectively. The design parameters for both controllers are chosen such that H_{∞_1} requires smaller control effort while H_{∞_2} requires bigger control effort, and their simulation results are compared with those of LQG_1 (smaller control effort) and LQG_3 (bigger control effort) controllers presented in Ref. [7], which use the same measurements $\mathbf{y} = [\ddot{x}_{1a}, \ddot{x}_{2a}, \ddot{x}_{3a}]^\mathrm{T}$ for feedback. Note that, unlike the proposed H_∞ control, the LQG algorithm takes into account control performance (response reduction) as the only objective in designing the controller. The weighting functions and other parameters used in the LMI computation for each controller are listed as follows: $\mathbf{W}_\mathbf{U} = (4.4s + 200)/(11s + 440)$, $\mathbf{W}_\mathbf{e} = (0.02s + 21,000)/(0.5s + 10)$, $\mathbf{W}_\mathbf{y} = (180s + 200)/(1.5s + 750)$, $\alpha = 0.1589$, $\beta = 0.1589$ and $\gamma_{\min} = 200$ for the H_{∞_1} controller; $\mathbf{W}_\mathbf{U} = (3.6s + 140)/(11s + 440)$, $\mathbf{W}_\mathbf{e} = (0.02s + 28,000)/(0.5s + 10)$, $\mathbf{W}_\mathbf{y} = (180s + 200)/(1.5s + 750)$, $\alpha = 0.1589$, $\beta = 0.1589$ and $\gamma_{\min} = 200$ for the H_{∞_2} controller. From the LMI-based

solution procedure, the resultant attenuation value γ is equal to 4134.9 and 3161.1 for the H_{∞_1} and H_{∞_2} controller, respectively. Consequently, two 15-state ($k = 15$) controllers are thus obtained, and they are further reduced to eight-state controller by the balanced-state reduction method [16] to facilitate implementation. The simulated responses using the H_{∞_1} and H_{∞_2} controllers under two earthquakes with 0.1 g PGA are tabulated in Columns (2)–(5) and Columns (11)–(14) of Table 2. In Table 2, the values inside the parentheses are the reduction percentages with respect to the "No Control" case presented in Table 1. As observed from Table 2, the reduction percentages of rms responses using the H_{∞_1} controller achieve about 50% with the control effort about 1000 kgf, while those using H_{∞_2} controller are further improved toward 60%, with the control effort about 1500 kgf. The reductions for the peak responses are relatively smaller and significant difference in peak value reduction is observed between the results from two different earthquakes. For comparison, the simulated responses using LQG_1 and LQG_3 controllers presented in Ref. [7] are also tabulated in Columns (6)–(9) and Columns (15)–(18) of Table 2. Based on the results, it is observed that the proposed H_∞ controllers have as effective performance as LQG controllers in controlling the frame building.

Table 2
Response quantities of actively controlled building using H_∞ controllers

	H_{∞_1}				LQG_1			
	El Centro (PGA = 0.1 g)		Kobe (PGA = 0.1 g)		El Centro (PGA = 0.1 g)		Kobe (PGA = 0.1 g)	
(1)	Peak (2)	rms (3)	Peak (4)	rms (5)	Peak (6)	rms (7)	Peak (8)	rms (9)
x_1 (cm)	1.395 (32.0)	0.293 (64.4)	2.010 (2.7)	0.308 (53.7)	1.415 (31.0)	0.307 (62.7)	1.970 (4.6)	0.318 (52.1)
x_2 (cm)	2.475 (45.9)	0.589 (66.7)	3.962 (11.8)	0.606 (57.6)	2.736 (40.4)	0.651 (63.1)	4.051 (9.8)	0.656 (54.1)
x_3 (cm)	3.002 (51.8)	0.706 (69.8)	4.972 (16.9)	0.746 (60.5)	3.339 (46.4)	0.802 (65.7)	5.240 (12.4)	0.827 (56.2)
$\ddot{x}_{1a}$ (g)	0.121 (29.0)	0.025 (50.5)	0.130 (40.0)	0.020 (48.5)	0.121 (29.0)	0.024 (52.9)	0.147 (31.9)	0.022 (45.0)
$\ddot{x}_{2a}$ (g)	0.159 (39.5)	0.034 (65.0)	0.177 (32.8)	0.031 (60.7)	0.166 (36.6)	0.037 (61.9)	0.192 (27.3)	0.035 (55.1)
$\ddot{x}_{3a}$ (g)	0.185 (50.2)	0.040 (68.7)	0.224 (40.3)	0.037 (64.2)	0.222 (40.2)	0.042 (66.9)	0.266 (29.1)	0.041 (60.2)
U (kgf)	1153	262	1782	275	1060	221	1424	224
	H_{∞_2}				LQG_3			
	El Centro (PGA = 0.1 g)		Kobe (PGA = 0.1 g)		El Centro (PGA = 0.1 g)		Kobe (PGA = 0.1 g)	
(10)	Peak (11)	rms (12)	Peak (13)	rms (14)	Peak (15)	rms (16)	Peak (17)	rms (18)
x_1 (cm)	1.289 (37.1)	0.255 (69.0)	1.813 (12.2)	0.274 (58.8)	1.339 (34.7)	0.261 (68.3)	1.924 (6.8)	0.288 (56.6)
x_2 (cm)	2.104 (54.2)	0.468 (73.5)	3.373 (24.9)	0.492 (65.6)	2.239 (51.2)	0.502 (71.6)	3.683 (18.0)	0.538 (62.3)
x_3 (cm)	2.270 (63.6)	0.544 (76.7)	4.062 (32.1)	0.589 (68.9)	2.653 (57.4)	0.604 (74.1)	4.557 (23.8)	0.663 (64.9)
$\ddot{x}_{1a}$ (g)	0.104 (39.3)	0.023 (55.8)	0.117 (46.1)	0.018 (54.6)	0.101 (40.9)	0.020 (60.8)	0.128 (40.7)	0.020 (50.0)
$\ddot{x}_{2a}$ (g)	0.149 (43.3)	0.029 (70.1)	0.135 (48.9)	0.024 (69.0)	0.133 (49.2)	0.027 (72.2)	0.157 (40.5)	0.026 (66.7)
$\ddot{x}_{3a}$ (g)	0.149 (59.9)	0.032 (75.2)	0.155 (58.7)	0.028 (73.2)	0.170 (54.2)	0.033 (74.0)	0.198 (47.2)	0.033 (68.0)
U (kgf)	1706	365	2632	390	1657	323	2430	351

4. Concluding remarks

The LMI-based H_∞ controllers that take into account robustness criteria have been introduced. Robustness criteria include performance robustness in reducing tracking error and in resistance to external disturbance and measurement noise, and the stability robustness with respect to system uncertainty. A numerical model of an experimental full-scale three-story seismic-excited building with an active bracing system, which has been verified through experiments in a literature by the same author, was used in the simulation to verify the applicability of the proposed controllers toward actual implementation. In the extensive simulations, two earthquakes, the 1940 El Centro and 1995 Kobe earthquakes, are used as the excitations to the building. The system uncertainty is assumed in the controller design and acceleration measurements are used as the feedback quantities for practical consideration. Two H_∞ controllers were designed to successfully demonstrate the flexibility of modulating control effort in this approach. Furthermore, the simulated results of H_∞ controllers are compared with those of LQG controllers for their effectiveness. From the simulated results, it was demonstrated that: (1) the LMI approach is efficient in computing the H_∞ controller; (2) the effectiveness of H_∞ controllers presented is remarkable and its robustness with respect to disturbance attenuation, tracking error, noise rejection and uncertainty is satisfactory; (3) the performances of H_∞ controllers are as effective as those of LQG controllers. Therefore, the LMI-based robust H_∞ control is suitable for application to civil engineering buildings for seismic protection.

Acknowledgements

The authors wish to express their gratitude to the National Science of Council, Taiwan, for the financial support under the grant number NSC 93-2745-E-032-007.

Appendix A

Derivation of Eqs. (15) and (16) (excerpted from Ref. [14])

Projection lemma: For a symmetric matrix $\mathbf{\Psi}$ and two matrices $\mathbf{P}$ and $\mathbf{Q}$, there exists a matrix $\boldsymbol{\theta}$ satisfying $\mathbf{\Psi}+\mathbf{P}^{\mathrm{T}}\boldsymbol{\theta}^{\mathrm{T}}\mathbf{Q}+\mathbf{Q}^{\mathrm{T}}\boldsymbol{\theta}\mathbf{P}<0$ if and only if $\mathbf{W}_{\mathbf{P}}^{\mathrm{T}}\mathbf{\Psi}\mathbf{W}_{\mathbf{P}}<0$ and $\mathbf{W}_{\mathbf{Q}}^{\mathrm{T}}\mathbf{\Psi}\mathbf{W}_{\mathbf{Q}}<0$, in which $\mathbf{W}_{\mathbf{P}}$ and $\mathbf{W}_{\mathbf{Q}}$ are the matrices whose columns are composed of the null space bases of $\mathbf{P}$ and $\mathbf{Q}$, respectively.

By the Projection lemma, the existence of a feasible $\boldsymbol{\theta}$ in inequality (12) requires the satisfaction of two conditions

$$\mathbf{W}_{\xi_{\mathbf{X}_{\mathbf{cl}}}}^{\mathrm{T}}\mathbf{\Psi}_{\mathbf{X}_{\mathbf{cl}}}\mathbf{W}_{\xi_{\mathbf{X}_{\mathbf{cl}}}}<0 \tag{A.1}$$

and

$$\mathbf{W}_{\psi}^{\mathrm{T}}\mathbf{\Psi}_{\mathbf{X}_{\mathbf{cl}}}\mathbf{W}_{\psi}<0, \tag{A.2}$$

in which $\mathbf{W}_{\xi_{\mathbf{X}_{\mathbf{cl}}}}$ and $\mathbf{W}_{\psi}$ are the matrices of null space bases of $\xi_{\mathbf{X}_{\mathbf{cl}}}$ and $\boldsymbol{\psi}$, respectively. In inequality (A.1), $\mathbf{X}_{\mathbf{cl}}$ appears in $\mathbf{\Psi}_{\mathbf{X}_{\mathbf{cl}}}$ and $\mathbf{W}_{\xi_{\mathbf{X}_{\mathbf{cl}}}}$ as well; therefore, it needs further manipulation as follows. From the observation that $\xi_{\mathbf{X}_{\mathbf{cl}}}$ can be expressed as

$$\xi_{\mathbf{X}_{\mathbf{cl}}}=\mathbf{\Phi}\begin{bmatrix}\mathbf{X}_{\mathbf{cl}} & 0 & 0\\ 0 & \mathbf{I}_{m_1} & 0\\ 0 & 0 & \mathbf{I}_{p_1}\end{bmatrix},\quad \mathbf{\Phi}=(\boldsymbol{\beta}^{\mathrm{T}},\ 0_{(k+m_2)\times m_1},\ \zeta_{12}^{\mathrm{T}}), \tag{A.3}$$

the null space matrices of $\xi_{\mathbf{X}_{\mathbf{cl}}}$ and $\mathbf{\Phi}$ are related by the equation

$$\mathbf{W}_{\xi_{\mathbf{X}_{\mathbf{cl}}}}=\begin{bmatrix}\mathbf{X}_{\mathbf{cl}}^{-1} & 0 & 0\\ 0 & \mathbf{I}_{m_1} & 0\\ 0 & 0 & \mathbf{I}_{p_1}\end{bmatrix}\mathbf{W}_{\mathbf{\Phi}}. \tag{A.4}$$

The substitution of Eq. (A.4) into inequality (A.1) leads to

$$\mathbf{W}_{\mathbf{\Phi}}^{\mathrm{T}}\mathbf{\Phi}_{\mathbf{X_{cl}}}\mathbf{W}_{\mathbf{\Phi}}<0 \tag{A.5}$$

in which

$$\mathbf{\Phi}_{\mathbf{X_{cl}}}=\begin{bmatrix}\mathbf{A}_0^{\mathrm{T}}\mathbf{X}_{\mathbf{cl}}^{-1}+\mathbf{X}_{\mathbf{cl}}^{-1}\mathbf{A}_0^{\mathrm{T}} & \mathbf{B}_0 & \mathbf{X}_{\mathbf{cl}}^{-1}\mathbf{C}_0^{\mathrm{T}}\\ \mathbf{B}_0^{\mathrm{T}} & -\gamma\mathbf{I} & \mathbf{D}_{11}^{\mathrm{T}}\\ \mathbf{C}_0\mathbf{X}_{\mathbf{cl}}^{-1} & \mathbf{D}_{11} & -\gamma\mathbf{I}\end{bmatrix}. \tag{A.6}$$

Now, we have obtained two inequalities (A.5) and (A.2), which guarantee the existence of a feasible $\mathbf{X_{cl}}$.

A further simplification of inequality (A.5) is performed by substituting the partition of $\mathbf{X_{cl}}$ and $\mathbf{X_{cl}^{-1}}$ expressed in Eq. (14) into $\mathbf{\Phi}_{\mathbf{X_{cl}}}$ in Eq. (A.6), i.e.,

$$\mathbf{\Phi}_{\mathbf{X_{cl}}}=\begin{bmatrix}\mathbf{AR}+\mathbf{RA}^{\mathrm{T}} & \mathbf{AM} & \mathbf{B}_1 & \mathbf{RC}_1^{\mathrm{T}}\\ \mathbf{M}^{\mathrm{T}}\mathbf{A}^{\mathrm{T}} & 0 & 0 & \mathbf{M}^{\mathrm{T}}\mathbf{C}_1^{\mathrm{T}}\\ \mathbf{B}_1^{\mathrm{T}} & 0 & -\gamma\mathbf{I} & \mathbf{D}_{11}^{\mathrm{T}}\\ \mathbf{C}_1\mathbf{R} & \mathbf{C}_1\mathbf{M} & \mathbf{D}_{11} & -\gamma\mathbf{I}\end{bmatrix} \tag{A.7}$$

and expressing the null space matrix $\mathbf{W}_{\mathbf{\Phi}}$ in inequality (A.5) as

$$\mathbf{W}_{\mathbf{\Phi}}=\begin{bmatrix}\mathbf{W}_1 & 0\\ 0 & 0\\ 0 & \mathbf{I}_{m_1}\\ \mathbf{W}_2 & 0\end{bmatrix}, \tag{A.8}$$

in which $\begin{bmatrix}\mathbf{W}_1\\ \mathbf{W}_2\end{bmatrix}=\mathbf{N_R}$ is the null space matrix of $[\mathbf{B}_2^{\mathrm{T}}\ \mathbf{D}_{12}^{\mathrm{T}}]$. By this, inequality (A.5) is rewritten as

$$\begin{bmatrix}\mathbf{W}_1 & 0\\ 0 & \mathbf{I}_{m_1}\\ \mathbf{W}_2 & 0\end{bmatrix}^{\mathrm{T}}\begin{bmatrix}\mathbf{AR}+\mathbf{RA}^{\mathrm{T}} & \mathbf{B}_1 & \mathbf{RC}_1^{\mathrm{T}}\\ \mathbf{B}_1^{\mathrm{T}} & -\gamma\mathbf{I} & \mathbf{D}_{11}^{\mathrm{T}}\\ \mathbf{C}_1\mathbf{R} & \mathbf{D}_{11} & -\gamma\mathbf{I}\end{bmatrix}\begin{bmatrix}\mathbf{W}_1 & 0\\ 0 & \mathbf{I}_{m_1}\\ \mathbf{W}_2 & 0\end{bmatrix}<0 \tag{A.9}$$

or rearranged as

$$\begin{bmatrix}\mathbf{N_R} & 0\\ 0 & \mathbf{I}_{m_1}\end{bmatrix}^{\mathrm{T}}\begin{bmatrix}\mathbf{AR}+\mathbf{RA}^{\mathrm{T}} & \mathbf{RC}_1^{\mathrm{T}} & \mathbf{B}_1\\ \mathbf{C}_1\mathbf{R} & -\gamma\mathbf{I} & \mathbf{D}_{11}\\ \mathbf{B}_1^{\mathrm{T}} & \mathbf{D}_{11}^{\mathrm{T}} & -\gamma\mathbf{I}\end{bmatrix}\begin{bmatrix}\mathbf{N_R} & 0\\ 0 & \mathbf{I}_{m_1}\end{bmatrix}<0. \tag{A.10}$$

In a similar manner, inequality (A.2) can be rewritten as

$$\begin{bmatrix}\mathbf{N_S} & 0\\ 0 & \mathbf{I}_{p_1}\end{bmatrix}^{\mathrm{T}}\begin{bmatrix}\mathbf{AS}+\mathbf{A}^{\mathrm{T}}\mathbf{S} & \mathbf{SB}_1 & \mathbf{C}_1^{\mathrm{T}}\\ \mathbf{B}_1^{\mathrm{T}}\mathbf{S} & -\gamma\mathbf{I} & \mathbf{D}_{11}^{\mathrm{T}}\\ \mathbf{C}_1 & \mathbf{D}_{11} & -\gamma\mathbf{I}\end{bmatrix}\begin{bmatrix}\mathbf{N_S} & 0\\ 0 & \mathbf{I}_{p_1}\end{bmatrix}<0, \tag{A.11}$$

in which $\mathbf{N_S}$ is the null space matrix of $[\mathbf{C}_2\ \mathbf{D}_{21}]$.

References

[1] T.T. Soong, *Active Structural Control: Theory and Practice*, Longman Scientific & Technical.

[2] T. Kobori, Y. Inoue, K. Seto, H. Iemura, A. Nishitani (Eds.) *Proceedings of Third World Conference on Structural Control*, Wiley, New York, 1998.

[3] F. Casciati (Ed.), *Proceedings of Third World Conference on Structural Control*, Wiley, New York, 2002.

[4] L.L. Chung, R.C. Lin, T.T. Soong, A.M. Reinhorn, Experiments on active control for MDOF seismic structures, *ASCE Journal of Engineering Mechanics* 115 (8) (1989) 1609–1627.

[5] S.J. Dyke, B.F. Spencer, A.E. Belknap, K.J. Ferrell, P. Quast, M.K. Sain, Absolute acceleration feedback control strategies for the active mass driver, *Proceedings of the 1st World Conference on Structural Control* 2 (1994) TP1-51–TP1-60.
[6] S.J. Dyke, B.F. Spencer, P. Quast, M.K. Sain, D.C. Kaspari, T.T. Soong, Experimental verification of acceleration feedback control strategies for an active tendon system, National Center for Earthquake Engineering Research Technical Report, NCEER-94-0024, 1994.
[7] J.C. Wu, Modeling of an actively braced full-scale building considering control–structure Interaction, *Earthquake Engineering and Structural Dynamics* 29 (2000) 1325–1342.
[8] J.C. Wu, B.C. Pan, Wind tunnel verification of actively controlled high-rise building in along-wind motion, *Journal of Wind Engineering and Industrial Aerodynamics* 90 (12–15) (2002) 1933–1950.
[9] J.C. Wu, L.Y. Cheng, Effects of attack angle on performance of actively controlled high-rise building motion, *Journal of Wind Engineering and Industrial Aerodynamics* 93 (5) (2005) 413–434.
[10] K. Zhou, J.C. Doyle, *Essentials of Robust Control*, Prentice-Hall, Englewood Cliffs, NJ, 1998.
[11] T. Basar, P. Bernhard, H_∞-*Optimal Control and Related Min–Max Design Problems—A Dynamic Game Approach*, Birkhauser, Boston, 1991.
[12] K. Glover, J.C. Doyle, State space formula for all stabilizing controllers that satisfy an H_∞-norm bound and relations to risk sensitivity, *System and Control Letters* 11 (1988) 167–172.
[13] J.C. Doyle, K. Glover, P. Khargonekar, B. Francis, State space solutions to standard H_2 and H_∞ control problems, *IEEE Transactions on Automatic Control* 34 (1989) 831–847.
[14] P. Gahinet, P. Apkarian, A linear matrix inequality approach to H_∞ control, *International Journal of Robust and Nonlinear Control* 4 (1994) 421–448.
[15] A. Packard, K. Zhou, P. Pandey, G. Becker, A collection of robust control problems leading to LMI's, *Proceedings of the 30th Conference on Decision Control*, Brighton, England.
[16] B.C. Moore, Principal component analysis in linear system: controllability, observability and model reduction, *IEEE Transactions on Automatic Control* 26 (1) (1987) 17–32.